Journal of Nuclear Medicine, published on July 26, 2017 as doi:10.2967/jnumed.117.193748

Targeted molecular radiotherapy of pediatric solid tumors using a radioiodinated alkyl-phospholipid ether analog

Running title: Alkyl-phospholipid ether radiotherapy

Dana C. Baiu[1], Ian R. Marsh[2], Alexander E. Boruch[1], Ankita Shahi[1], Saswati Bhattacharya[1], Justin J. Jeffery[3], Qianqian Zhao[4], Lance T. Hall[3], Jamey P. Weichert[2,3], Bryan P. Bednarz[2], Mario Otto[1]*

[1]Department of Pediatrics, Carbone Cancer Center, [2]Department of Medical Physics, [3]Department of Radiology, and [4]Department of Biostatistics and Medical Informatics, School of Medicine and Public Health, University Wisconsin-Madison, Madison, WI, USA

Keywords: targeted radiotherapy, pediatric cancer, radionuclide therapy, microPET/CT imaging

Abbreviations: %ID/g, percent injected dose per gram; CT, computed tomography; MIBG, metaiodobenzylguanidine; NSG, NOD.Cg-Prkdc^{scid} Il2rg^{tm1Wjl}/SzJ; PET, positron emission tomography.

Grant support: NIH R21CA198392-01, the Midwest Athletes against Childhood Cancer Foundation, Hyundai Hope on Wheels, SU2C/St. Baldrick's Pediatric

Dream Team Translational Research Grant SU2C-AACR-DT1113 and NIH/NCI P30 CA014520.

*__Corresponding author__: Mario Otto, Department of Pediatrics, WIMR 4153, 1111 Highland Avenue, Madison WI 53705; +1-608-265-9645; motto@pediatrics.wisc.edu

First author: Dana C. Baiu, Department of Pediatrics, 1111 Highland Avenue, Madison WI 53705; +1-608-263-7591; dcbaiu@pediatrics.wisc.edu

ABSTRACT

External beam radiotherapy plays a critical role in the treatment of most pediatric solid tumors. Particularly in children, achieving an optimal therapeutic index to avoid damage to normal tissue is extremely important. Consequently, in metastatic disease, the utility of external beam radiotherapy is very limited. Molecular radiotherapy with tumor-targeted radionuclides may overcome some of these challenges, but to date no single cancer selective agent exists, capable of treating various pediatric malignancies independent of their histopathological origin. We tested the therapeutic potential of the clinical-grade alkyl-phospholipid ether analog CLR1404 as scaffold for tumor-targeted radiotherapy of pediatric malignancies. **Methods**: Uptake of CLR1404 by pediatric solid tumor cells was tested in vitro, by flow cytometry, and in vivo, by positron emission tomography (PET)/computed tomography (CT) imaging and dosimetry. The therapeutic potential of ^{131}I-CLR1404 was evaluated in xenograft models. **Results:** In vitro, fluorescent CLR1404-BODIPY showed significant selective uptake in a variety of pediatric cancer lines compared to normal controls. In vivo tumor-targeted uptake in mouse xenograft models using ^{124}I-CLR1404 was confirmed by imaging. Single-dose intravenous injection of ^{131}I-CLR1404 significantly delayed tumor growth in all rodent pediatric xenograft models and extended animal survival, while demonstrating a favorable side effect profile. **Conclusion**: ^{131}I-CLR1404 has the potential to become a tumor-targeted radiotherapeutic drug with broad applicability in pediatric oncology. Since ^{131}I-CLR1404 has entered clinical trials in adults, our data warrants the development of pediatric clinical trials for this particularly vulnerable patient population.

INTRODUCTION

External beam radiation therapy plays an indispensable role in the context of both curative and palliative treatment approaches for managing pediatric solid cancers (*1,2*). Although a majority of pediatric solid cancers are radiosensitive, for children with tumors that are less radiosensitive, not amenable to surgical bulk reduction, or in the context of minimal residual disease, high doses or large areas of exposure to radiation are required to achieve a therapeutic effect (*2-4*). Consequently, normal tissue undergoing growth and development is exposed to and damaged by the effect of off-target radiation, often with sequelae that impair the health of an affected individual for a lifetime (*2,4*). For this reason, external beam radiotherapy is not feasible in children with widely metastatic cancer, and is only used to treat primary or particularly bulky metastatic tumors.

For these difficult cases, targeted molecular radiotherapy using systemic administration of radionuclides, such as the beta-emitting ^{131}I, may be effectively used to deliver sufficient cytotoxic radioactivity to cancer cells (*5*). Due to the relatively short range in soft tissues of the radiation emitted during decay, beta emitters insure large energy deposition in small volumes of tissue on a cellular and multicellular scale. One such example of beta emitter-radiolabeled targeting moiety that has been successfully utilized in pediatric radiotherapy for several decades is metaiodobenzylguanidine (MIBG), a sympathomimetic guanethidine derivative (*6*). Both as monotherapy (often in the palliative setting), or in combination with chemotherapy and autologous stem cell transplant in curative approaches, systemic administration of ^{131}I-MIBG is an effective therapy in neuroblastoma, with response rates of up to 46% (*7*). However, ^{131}I-MIBG

therapy is not possible in approximately 10% of neuroblastoma tumors since they do not incorporate MIBG. Other devastating pediatric solid cancers, such as rhabdomyosarcoma, Ewing's sarcoma, osteosarcoma, do not express a widely targetable marker for molecular radiotherapy. Hence, even with standard multimodality therapy, most pediatric patients with metastatic or relapsed solid tumors are confronted with a poor prognosis. The chance of cure for high-risk neuroblastoma is approximately 50%, and for children with primary or relapsed metastatic rhabdomyosarcoma it is less than 25%; patients with recurrent Ewing's sarcoma have an overall survival of less than 10% (*8-10*). These statistics underscore the need for developing new therapeutic agents, preferably with cancer-specific uptake and broad applicability for these particularly hard-to-cure malignancies.

CLR1404, 18-(p-iodophenyl) octadecyl phosphocholine, is an iodinated phospholipid ether analog with selective sequestration in cancer cells. CLR1404 enters cells preferentially via lipid rafts, which are overexpressed in the plasma membrane of cancer cells relative to normal cells, leading to remarkable tumor selectivity (*11*). CLR1404 uptake has been confirmed in more than 60 adult cancer cell lines, xenograft models, and patient-derived tissues, including cancer stem cells, with little uptake in normal cells (*11,12*). CLR1404 has entered clinical trials in adults as a PET/CT imaging agent (labeled with ^{124}I) and for radiotherapy (labeled with ^{131}I, physical properties detailed in Supplemental Table 1) (*13,14*). In addition, we have recently reported the potential of CLR1404 to specifically target and exert an anti-cancer effect against pediatric neuroblastoma both in vitro, and in vivo in murine xenograft models (*12*), with no detectable

hematotoxicity, or adverse effects on the animal health status. The favorable toxicological profile of CLR 1404 following parenteral administration (*12,15*) and its broad cancer-targeting ability (*11*) recommend CLR1404 as a carrier for ^{131}I radiotherapy in disseminated disease.

Many critical differences exist between pediatric and adult solid tumors. While the vast majority of pediatric cancers have an embryonal origin, i.e. are derived from early-differentiating, feto-embryonal tissues, most adult solid tumors are rather derived from mature, epithelial tissues (*16*). Genetic analyses of pediatric cancers demonstrate many differences when compared to adult cancers, making pediatric cancers distinct diseases (*17*), which require different treatment strategies with completely different outcomes when compared to adults. In this study, we tested the hypothesis that the preferential uptake of CLR1404 by cancer cells may be exploited for molecularly targeted radiotherapy of pediatric solid tumors, in vivo, using xenograft models of neuroblastoma, rhabdomyosarcoma, Ewing's sarcoma and osteosarcoma.

MATERIALS AND METHODS

Cells

Alveolar rhabdomyosarcoma cell lines Rh30, Rh41 and Ewing's sarcoma cell lines TC-71, TC-106 (kindly provided by Children's Oncology Group Cell Repository, Lubbock, TX), neuroblastoma cell lines CHLA-20, NB-1691 (courtesy of Dr. Andrew Davidoff, St. Jude Children's Research Hospital, Memphis, TN), osteosarcoma cell line SAOS-2, embryonal rhabdomyosarcoma cell line RD (ATCC, Manassas, VA), and primary cultures of normal human fibroblasts (kind

gift from Dr. V. Browning, University of Wisconsin-Madison), were cultured as previously described (*12,18*).

CLR1404 Synthesis and Radioiodination

18-(p-iodophenyl) octadecyl phosphocholine (known as NM404, or CLR1404), its radioactive analogs ^{124}I-CLR1404 and ^{131}I-CLR1404 (carrying ^{124}I, or ^{131}I, instead of the stable ^{127}I), and fluorescently labeled CLR1404-BODIPY (where ^{127}I was replaced with the fluorescent tag BODIPY FL), were kindly provided by Cellectar Biosciences, Madison, WI. Clinical grade CLR1404 was radiolabeled with ^{124}I or ^{131}I (Supplemental Table 1) using an isotope exchange reaction with sodium iodide as published previously (*11*). Isolated radiochemical yields for radio-iodinated ^{131}I-CLR1404 prepared under cGMP-manufacturing guidelines were consistently above 70% and radiochemical purity exceeded 96% in all cases. The mean specific activity was 18.5 x10^8 MBq/mol (range 7.4-25.9x10^8 MBq/mol).

In Vitro Uptake of CLR1404-BODIPY

Green fluorescence of cells (5×10^5 cells/ml) after culture for 18 hours with 5 μM of fluorescent derivative CLR1404-BODIPY (*11*) was assessed by flow cytometry (MACSQuant Analyzer, Miltenyi Biotec, Auburn, CA) and analyzed using FlowJo 9.2 (FlowJo LLC, Ashland, OR). Mean fluorescence intensity was corrected for differences in cell size by normalizing to autofluorescence.

Xenograft Models

Animal care and use were in compliance with institutional review board approved protocols and NIH guidelines. Human tumor xenografts were established in NOD.Cg-Prkdc^{scid} Il2rg^{tm1Wjl}/SzJ mice (Jackson Laboratory, Bar Harbor, ME), hereafter abbreviated NSG, by inoculating 2x10^6 tumor cells in 200 µl 3 mg/ml Matrigel (BD Biosciences, San José, CA) subcutaneously in the flank. Radioiodinated CLR1404 was administered intravenously when average tumor volumes reached ~150 mm^3. Injected doses were calculated from the difference in counts of syringes prior to and after injection. Animals were housed individually in cages shielded by lead sheets to avoid cumulative irradiation.

PET/CT Imaging and Dosimetry with ^{124}I-CLR1404

Mice were administered on average 371 MBq/kg bodyweight ^{124}I-CLR1404 (range 296-500 MBq/kg) intravenously and were scanned on an Inveon microPET/CT (Siemens, Knoxville, TN) at 1, 24, 48, 72 hours, with additional scans at 96, 144 or 168 hours post-injection, while anesthetized under 2% isoflurane. The energy window for ^{124}I was set at 250-650 keV and each mouse was scanned until 40 million counts were collected to achieve optimal signal to noise characteristics. The counts were binned in three-dimensional histograms and the resulting images were reconstructed using ordered-subset expectation maximization followed by maximum a posteriori algorithm. All data were reconstructed without scatter correction. Following the imaging the PET/CT data were pre-processed, and organ and tumor regions of interest were contoured using the AMIRA software (FEI/Thermo Fisher Scientific, Berlin,

Germany). The imaging data was then imported into a Monte Carlo-based mouse-specific dosimetry software (*14,19*), to perform three-dimensional dose calculations. The CT and the PET images were used in the Monte Carlo simulation to define the geometry and source distribution, respectively. The radioactivity of the ^{124}I-CLR1404 was converted to the radioactivity of ^{131}I-CLR1404 at each time point by assuming the same injection activity and accounting for the difference in physical decay rates. Mean absorbed doses to normal organs and tumor from ^{131}I-CLR1404 were estimated for each mouse.

Molecular Radiotherapy with ^{131}I-CLR1404

Mice bearing xenografts (6-9 animals/group, as detailed in Table 1) were injected with a mean dose ± standard deviation of 115 ± 30 MBq/kg bodyweight ^{131}I-CLR1404 (range: 100-180 MBq/kg) or an equivalent amount of control non-radioactive CLR1404 (excipient) into the lateral tail vein, and tumor growth was monitored twice weekly. A health score was calculated based on a 5 clinical criteria evaluation system (modified from (*20*), by scoring with grades of 0, -1, and -2 the animal posture, activity, fur texture, weight loss (<10%, >10% <20%, or >20%) and skin integrity, summed to a final score between 0, normal, and -10, severe health impairment. To determine treatment-related hematotoxicity in immunocompetent mice, peripheral blood samples of five ^{131}I-CLR1404-treated (mean treatment dose ± standard deviation of 115 ± 4 MBq/kg bodyweight, range 111-122 MBq/kg) BALB/c mice (Jackson Laboratory) were collected before treatment and 2, 4 and 6 weeks post-treatment, and evaluated for platelet and erythrocyte counts, hemoglobin concentration and leucocyte differential analysis

on a VETScan HM5 hematology analyzer (Abaxis, Union City, CA).

Statistical Analysis

Tumor growth was analyzed and compared between the two experimental groups by a linear mixed effects model using SAS software (SAS Institute Inc., Cary, NC), with the group as the fixed effect and the animal as random effect (to account for repeated measures for the same animals) and the log-transformed tumor volume used as the outcome measure (*21*). Comparisons between groups were done using t-test. Kaplan-Meier survival curves were used to depict the time to tumors reaching/exceeding 4,000 mm^3, set as criterion for euthanasia.

Results

Pediatric Solid Cancer Cells Take Up and Retain CLR1404

Using green fluorescent BODIPY-labeled CLR1404, we determined its accumulation in various pediatric solid cancer cell lines by flow cytometry. CLR1404-BODIPY was previously shown to display similar tumor uptake and retention to the radioiodinated CLR1404 analogs (*11*). All tested cell lines sequestered and retained significantly higher amounts of CLR1404-BODIPY (average 6.6 fold higher, range 5.6-7.3) when compared to uptake by human primary normal cell cultures (Fig. 1), corroborating our previously published results (*11*). Uptake varied between cell lines and cancer types.

^{124}I-CLR1404 Targets Pediatric Solid Cancer Cells in Vivo

In vivo uptake and retention of ^{124}I-CLR1404 in tumors was evaluated by microPET/CT in NSG mice bearing human xenografts (four mice for each tumor cell line: Rh30, TC-71, CHLA-20 and NB-1691). The distribution of ^{124}I-CLR1404 in tissues showed preferential accumulation in human cancer cell xenografts 72 hours post-intravenous administration (Fig. 2) reaching %ID/g values of 7-12% in rhabdomyosarcoma xenografts Rh-30, 3-6% ID/g in Ewing's sarcoma TC-71, 3-9% ID/g in neuroblastoma tumors CHLA-20, and 4-7% in NB-1691 xenografts. While ^{124}I-CLR1404 was detected in the blood pool at high levels at 1 and 24 hours after injection (evidenced in %ID/g values determined in the heart) it subsequently decreased in normal tissues, in parallel with its accumulation in tumors (Supplemental Tables 2-5). In normal tissues, the activity remained mostly detectable in organs with high blood flow such as the heart, lungs, liver and spleen, consistent with other small animal biodistribution studies.

Calculated Cumulative Absorbed Dose of ^{131}I-CLR1404 in Xenografts

The estimated cumulative absorbed doses from ^{131}I-CLR1404 were calculated using mouse-specific imaging data (Fig. 3). The largest cumulative absorbed dose delivered to a specific xenograft was calculated in the rhabdomyosarcoma Rh30 xenograft mice, where the average dose was 2.4 ± 0.42 Gy/MBq. Average cumulative absorbed doses of 1.21 ± 0.53 Gy/MBq and 1.10 ± 0.25 Gy/MBq were calculated in the case of the NB-1691 and CHLA-20 xenografts. The lowest cumulative absorbed dose was calculated in the Ewing's sarcoma TC-71 tumors, where the average dose was 0.92 ± 0.15 Gy/MBq.

^{131}I-CLR1404 Slows Growth of Pediatric Solid Cancer Xenografts and Improves Survival of Xenografted Animals

To test and exploit the cancer-targeting capacity of this new drug for radiotherapeutic purposes in pediatric cancers, groups of 6-8 xenograft-bearing mice were treated with a single dose of clinical-grade ^{131}I-CLR1404. The single-dose treatment significantly slowed tumor growth of all four pediatric solid cancer types tested, when compared to control animals treated with excipient containing the equivalent amount of non-radioactive CLR1404 (Fig. 4, Table 1 and Supplemental Figs. 1-3). The evaluation of individual tumor growth patterns indicates that starting one week after initiation of treatment, mice treated with ^{131}I-CLR1404 have on average 2-3 fold smaller tumors than excipient-treated animals (for Ewing's sarcoma, rhabdomyosarcoma and osteosarcoma xenografts), or at least 1,000mm^3 smaller than excipient-treated animals (for neuroblastoma tumors). The in vivo data support a strong therapeutic effect of ^{131}I-CLR1404 over aggressive tumor growth rates during the first 3 to 4 weeks post-treatment (corresponding to up to four ^{131}I half-lives). The treatment of xenografted mice with ^{131}I-CLR1404 led to an extension of the median survival, statistically significant for animals xenografted with Ewing's sarcoma and rhabdomyosarcoma (Fig. 5 and Supplemental Fig.4).

Molecular Radiotherapy Using ^{131}I-CLR1404 Does Not Induce Overt Radiotoxicity

Radiotoxicity was monitored in all NSG mice bearing sarcoma xenografts. The majority of the animals continued to gain weight during the 30-60 days

observation period (Supplemental Fig. 5A). The animals showed no signs of severe acute or chronic morbidity, with health score minimums averaging -3 (median -3.5, on a scale of 0 to -10) between weeks 2 and 4 post-treatment, but normalizing afterwards (Supplemental Fig. 5B, Ewing's sarcoma, rhabdomyosarcoma), except for one animal in the TC-106 Ewing's sarcoma group. Weight loss as an indication of systemic radiation toxicity was observed during the first 3 weeks of radiotherapy in 65% of NSG mice (average maximum weight loss of 5.3% across all ^{131}I-CLR1404 treated mice) and was the single most important health criterion decreasing the animal health scores (Supplemental Fig. 5B). In wild type animals, health scores were zero (unaffected), and average blood counts and hemoglobin concentration were maintained into normal ranges after treatment with the same doses of ^{131}I-CLR1404 as the tumor-bearing animals (Supplemental Figs. 5C and 5D), suggesting an acceptable therapeutic index for ^{131}I-CLR1404.

Discussion

Our results indicate that CLR1404 is an efficient cancer-targeting molecule in pediatric solid cancers, with minor uptake in normal tissues. The preferential uptake of CLR1404 and its radioactive analogs in cancer cells is extremely important for both diagnostic imaging and radiotherapy in these difficult-to-cure pediatric malignancies, particularly in the setting of primary disseminated disease or relapse. Few radiolabeled compounds are available in pediatric oncology tumor detection and therapy, and most of them are utilized for diagnostic imaging. Positron emission tomography with ^{18}F-deoxyglucose, in

combination with PET/CT has advanced as the most widely used functional diagnostic imaging tool for a broad variety of pediatric solid tumors (*22*). However, high glucose-consumption by brain or inflammatory cells results in ^{18}F-deoxyglucose uptake, and can obscure tumor tissue or lead to false positive results, an important limitation of this imaging modality (*22*). ^{123}I-MIBG scintigraphy is routinely prescribed for initial diagnosis, staging and response assessment in neuroblastoma. Other theranostic radioactive small molecules are being developed and are in clinical testing, such as DOTATATE for neuroendocrine tumors, including neuroblastoma (*23,24*). ^{131}I-MIBG for the treatment of neuroblastoma is perhaps currently the only widely accepted, targeted molecular radiotherapy, available at specialized treatment centers with suitable infrastructure. In osteosarcoma, ^{153}Sm-ethylenediamine-tetramethylene-phosphonic acid is available for the palliative treatment of bone lesions (*25*). In stark contrast to these targeted radiotherapeutic molecules, CLR1404 and its radioactive analogs target a much wider array of cancer types and tumors of practically every tissue origin, including neuroblastoma, rhabdomyosarcoma, Ewing's sarcoma, and osteosarcoma, a characteristic that emphasizes its broad applicability in targeting pediatric solid cancers. Broad applicability is paramount in pediatric oncology, from a drug development and regulatory standpoint, given the rarity of cases per tumor type, patient variability in targetable markers, and recoverable costs for pre-clinical and clinical development. The latter is a major barrier for the pediatric-specific development of anticancer treatments by the pharmaceutical industry, reflected by the fact that few drugs have been developed in the last 20 years specifically to treat pediatric cancers (*26*).

Paralleling the in vitro CLR1404 uptake results, we observed differences in tumor-specific absorbed doses between the three cancer types in vivo. The %ID/g of ^{124}I that accumulated in our tumor xenografts using CLR1404 as carrier was higher than observed for instance with MIBG. Seo et al. reported a %ID/g uptake of ^{124}I carried by MIBG of less than 2% in mouse subcutaneous human neuroblastoma xenografts overexpressing human norepinephrine transporter. In their study, %ID/g of ^{124}I was higher in tumors implanted under the renal capsule but did not exceed on average 3-4% after the first 24 hours, with rapid decline thereafter (*27*). However, we did not perform a direct comparison between ^{124}I-MIBG and ^{124}I-CLR1404 in neuroblastoma xenograft models, which limits our ability to compare the two carriers.

The selective uptake and retention of ^{131}I-CLR1404 in tumors was ascertained by dosimetry, biodistribution and pharmacokinetic studies in the context of two completed clinical trials in adults with advanced solid cancers (*13,28*). As we have previously shown, ^{124}I-CLR1404 is an ideal agent for pre-treatment dosimetry in the pre-clinical and clinical setting (*14,19*) and thus may allow the calculation and prescription of personalized, patient-specific doses, as is currently routine for external beam irradiation (*29*). This is particularly important given the variety of tumors that can potentially be treated with ^{131}I-CLR1404, the expected variability in tumor- or patient-specific absorbed doses, and will allow for important optimization of the therapeutic ratio, which is of great concern specifically in the pediatric setting. Such applications are supported by previous observations in clinical setting indicating that imaging using 0.02 mg/kg body

weight ^{124}I-CLR1404 would not prevent therapeutic doses of ^{131}I-CLR1404 from entering tumors (*30*).

The capacity of ^{131}I-CLR1404 to deliver effective radiation doses to a variety of pediatric solid cancer xenografts has the potential to profoundly impact the clinical management of these patients in the near future. Administration of a single dose with mean activity of 115 MBq/kg bodyweight ^{131}I-CLR1404, although not curative, demonstrated statistically significant therapeutic activity in all four types of pediatric solid tumors tested (Table 1; Fig. 4). Notably, all cell lines utilized to establish xenografts in this study are derived from highly aggressive human tumors that are post-chemotherapy, multidrug-resistant and bear markers of aggressiveness such as MYCN-amplification (NB-1691) (*31*), non-functional p53 (TC-71) or chromosomal translocations (Rh30) (*32*). By estimating the cumulative absorbed doses through quantitative imaging, we determined that doses of 0.5-2.8 Gy/MBq were delivered to solid tumor xenografts with our one-time, non-optimized dose of molecular-targeted radiotherapy. Compared to single fraction, external beam radiation therapy, these doses would be considered suboptimal in controlling heterotopic solid tumor xenografts in immunodeficient mouse models. Our study was not geared towards therapy optimization, but rather designed to show first proof-of-principle in the pre-clinical setting. Owing to a specific genetic defect in the *Prkdc* gene which is involved in DNA damage repair, the NSG mouse strain is markedly radiosensitive, but allows the reliable xenotransplantation of a broad variety human cancer tissues due to the profound immunosuppression (*33*). This enabled us to establish an array of pediatric cancer xenograft models, but we chose to limit the injected radioactivity to avoid

excessive tissue radiotoxicity while accepting decreased therapeutic effects. We have previously published data on adult tumor xenograft models in other immunodeficient mouse strains, in which single doses of up to 200 MBq/kg bodyweight of ^{131}I-CLR1404 were administered, leading to significant tumor shrinkage and even cure of some animals in certain cancer types (*11*).

In this context, recent results of a phase I multi-center open-label pilot study in 10 adult patients with relapsed or refractory advanced solid malignancies are encouraging, showing disease stabilization in 40% of the patients receiving ^{131}I-CLR1404 therapy (*13,28*) at the maximum dose administered of 1387 MBq/m^2 (approximately 30 MBq/kg). This dose is considerably lower than prescribed in the context of ^{131}I-MIBG therapy in children with neuroblastoma (on average 450-550 MBq/kg), in which transient thrombocytopenia or neutropenia are expected, and are alleviated by platelet transfusion or growth factor treatment (e.g. with filgrastim), and for higher radioactive doses, autologous stem cell support (*6*). However, since the pharmacokinetic properties of CLR1404 (*13,34*) differ from MIBG (*35*), only a clinical study can clarify the maximum tolerated dose of this compound in children. We therefore believe that in a clinical trial with appropriate supportive care, higher doses of ^{131}I-CLR1404 could be tolerated than we have tested in our pre-clinical mouse model, and ultimately might improve the anti-tumor effects.

CONCLUSIONS

Our data indicate that ^{131}I-CLR1404 is an effective and well-tolerated molecular-targeted radiotherapeutic agent in mouse models of high-risk pediatric

solid cancers that have a particular dismal outcome in patients with relapsed, refractory or disseminated disease. While a pediatric clinical trial is in development at our institution, future pre-clinical research will be geared towards integrating ^{131}I-CLR1404 in multimodality therapy approaches, in combination with chemotherapy, external beam radiotherapy, or immunotherapy.

ACKNOWLEDGEMENTS

We acknowledge NIH R21CA198392-01, NIH/NCI P30CA014520, and we thank the Midwest Athletes against Childhood Cancer Foundation, Hyundai Hope on Wheels, SU2C/St. Baldrick's Pediatric Dream Team Translational Research Grant SU2C-AACR-DT1113 for their support.

DISCLAIMER

J.P.W. was co-founder of Cellectar Biosciences. No other interests to declare.

REFERENCES

1. Wolden SL, Anderson JR, Crist WM, et al. Indications for radiotherapy and chemotherapy after complete resection in rhabdomyosarcoma: a report from the intergroup rhabdomyosarcoma studies I to III. *J Clin Oncol.* 1999;17:3468-3475.

2. Laverdiere C, Cheung NK, Kushner BH, et al. Long-term complications in survivors of advanced stage neuroblastoma. *Pediatr Blood Cancer.* 2005;45:324-332.

3. Indelicato DJ, Keole SR, Shahlaee AH, Shi W, Morris CG, Marcus RB, Jr. Definitive radiotherapy for Ewing tumors of extremities and pelvis: long-term disease control, limb function, and treatment toxicity. *Int J Radiat Oncol Biol Phys.* 2008;72:871-877.

4. Spix C, Pastore G, Sankila R, Stiller CA, Steliarova-Foucher E. Neuroblastoma incidence and survival in European children (1978-1997): report from the Automated Childhood Cancer Information System Project. *Eur J Cancer.* 2006;42:2081-2091.

5. Schmidt M, Baum RP, Simon T, Howman-Giles R. Therapeutic nuclear medicine in pediatric malignancy. *Q J Nucl Med Mol Imaging.* 2010;54:411-428.

6. Parisi MT, Eslamy H, Park JR, Shulkin BL, Yanik GA. (1)(3)(1)I-Metaiodobenzylguanidine theranostics in neuroblastoma: historical perspectives; practical applications. *Semin Nucl Med.* 2016;46:184-202.

7. Polishchuk AL, DuBois SG, Haas-Kogan D, Hawkins R, Matthay KK. Response, survival, and toxicity after iodine-131-metaiodobenzylguanidine therapy for neuroblastoma in preadolescents, adolescents, and adults. *Cancer.* 2011;117:4286-4293.

8. Lager JJ, Lyden ER, Anderson JR, Pappo AS, Meyer WH, Breitfeld PP. Pooled analysis of phase II window studies in children with contemporary high-risk metastatic rhabdomyosarcoma: a report from the Soft Tissue Sarcoma Committee of the Children's Oncology Group. *Journal Clin Oncol.* 2006;24:3415-3422.

9. Bacci G, Ferrari S, Longhi A, et al. Therapy and survival after recurrence of Ewing's tumors: the Rizzoli experience in 195 patients treated with adjuvant

and neoadjuvant chemotherapy from 1979 to 1997. *Ann Oncol.* 2003;14:1654-1659.

10. Park JR, Bagatell R, London WB, et al. Children's Oncology Group's 2013 blueprint for research: neuroblastoma. *Pediatr Blood Cancer.* 2013;60:985-993.

11. Weichert JP, Clark PA, Kandela IK, et al. Alkylphosphocholine analogs for broad-spectrum cancer imaging and therapy. *Sci Transl Med.* 2014;6:240ra275.

12. Marino R, Baiu DC, Bhattacharya S, et al. Tumor-selective anti-cancer effects of the synthetic alkyl phosphocholine analog CLR1404 in neuroblastoma. *Am J Cancer Res.* 2015;5:3422-3435.

13. Grudzinski JJ, Titz B, Kozak K, et al. A phase 1 study of 131I-CLR1404 in patients with relapsed or refractory advanced solid tumors: dosimetry, biodistribution, pharmacokinetics, and safety. *PLoS One.* 2014;9:e111652.

14. Besemer A, Grudzinski J, Titz B, Bednarz JB. Evaluation of dosimetric uncertainties in individualized targeted radionuclide therapy (TRT) treatment planning using pre-clinical data. *Medical Physics.* 2015;42:3675-3675.

15. Jiang H, Cannon MJ, Banach M, et al. Quantification of CLR1401, a novel alkylphosphocholine anticancer agent, in rat plasma by hydrophilic interaction liquid chromatography-tandem mass spectrometric detection. *J Chromatogr B Analyt Technol Biomed Life Sci.* 2010;878:1513-1518.

16. Simone JV, Lyons J. The evolution of cancer care for children and adults. *J Clin Oncol.* 1998;16:2904-2905.

17. Downing JR, Wilson RK, Zhang J, et al. The Pediatric Cancer Genome Project. *Nat Genet.* 2012;44:619-622.

18. Kang MH, Smith MA, Morton CL, Keshelava N, Houghton PJ, Reynolds CP. National Cancer Institute pediatric preclinical testing program: model description for in vitro cytotoxicity testing. *Pediatr Blood Cancer.* 2011;56:239-249.

19. Morris ZS, Weichert JP, Saker J, et al. Therapeutic combination of radiolabeled CLR1404 with external beam radiation in head and neck cancer model systems. *Radiother Oncol.* 2015;116:504-509.

20. Cooke KR, Kobzik L, Martin TR, et al. An experimental model of idiopathic pneumonia syndrome after bone marrow transplantation: I. the roles of minor H antigens and endotoxin. *Blood.* 1996;88:3230-3239.

21. Laird NM, Ware JH. Random-effects models for longitudinal data. *Biometrics.* 1982;38:963-974.

22. Uslu L, Donig J, Link M, Rosenberg J, Quon A, Daldrup-Link HE. Value of 18F-FDG PET and PET/CT for evaluation of pediatric malignancies. *J Nucl Med.* 2015;56:274-286.

23. Kong G, Hofman MS, Murray WK, et al. Initial experience with gallium-68 DOTA-octreotate PET/CT and peptide receptor radionuclide therapy for pediatric patients with refractory metastatic neuroblastoma. *J Pediatr Hematol Oncol.* 2016;38:87-96.

24. Gains JE, Bomanji JB, Fersht NL, et al. 177Lu-DOTATATE molecular radiotherapy for childhood neuroblastoma. *J Nucl Med.* 2011;52:1041-1047.

25. Anderson P, Nunez R. Samarium lexidronam (153Sm-EDTMP): skeletal radiation for osteoblastic bone metastases and osteosarcoma. *Expert Rev Anticancer Ther.* 2007;7:1517-1527.

26. Adamson PC. Improving the outcome for children with cancer: development of targeted new agents. *CA Cancer J Clin.* 2015;65:212-220.

27. Seo Y, Gustafson WC, Dannoon SF, et al. Tumor dosimetry using [124I]m-iodobenzylguanidine microPET/CT for [131I]m-iodobenzylguanidine treatment of neuroblastoma in a murine xenograft model. *Mol Imaging Biol.* 2012;14:735-742.

28. Lubner SJ, Mullvain J, Perlman S, et al. A phase 1, multi-center, open-label, dose-escalation study of 131I-CLR1404 in subjects with relapsed or refractory advanced solid malignancies. *Cancer Invest.* 2015;33:483-489.

29. McGowan DR, Guy MJ. Time to demand dosimetry for molecular radiotherapy? *Brit J Radiol.* 2015;88:20140720-20140723.

30. Grudzinski JJ, Burnette RR, Weichert JP, Jeraj R. Dosimetric effectiveness of targeted radionuclide therapy based on a pharmacokinetic landscape. *Cancer Biother Radiopharm.* 2010;25:417-426.

31. He J, Gu LB, Zhang HL, Zhou MX. Crosstalk between MYCN and MDM2-p53 signal pathways regulates tumor cell growth and apoptosis in neuroblastoma. *Cell Cycle.* 2011;10:2994-3002.

32. Rodriguez-Perales S, Martinez-Ramirez A, de Andres SA, et al. Molecular cytogenetic characterization of rhabdomyosarcoma cell lines. *Cancer Genet Cytogen.* 2004;148:35-43.

33. Shultz LD, Banuelos S, Lyons B, et al. NOD/LtSz-Rag1nullPfpnull mice: a new model system with increased levels of human peripheral leukocyte and hematopoietic stem-cell engraftment. *Transplantation.* 2003;76:1036-1042.

34. Grudzinski JJ, Floberg JM, Mudd SR, et al. Application of a whole-body pharmacokinetic model for targeted radionuclide therapy to NM404 and FLT. *Phys Med Biol.* 2012;57:1641-1657.

35. Ehninger G, Klingebiel T, Kumbier I, et al. Stability and pharmacokinetics of m-[131I]iodobenzylguanidine in patients. *Cancer Res.* 1987;47:6147-6149.

FIGURES AND LEGENDS

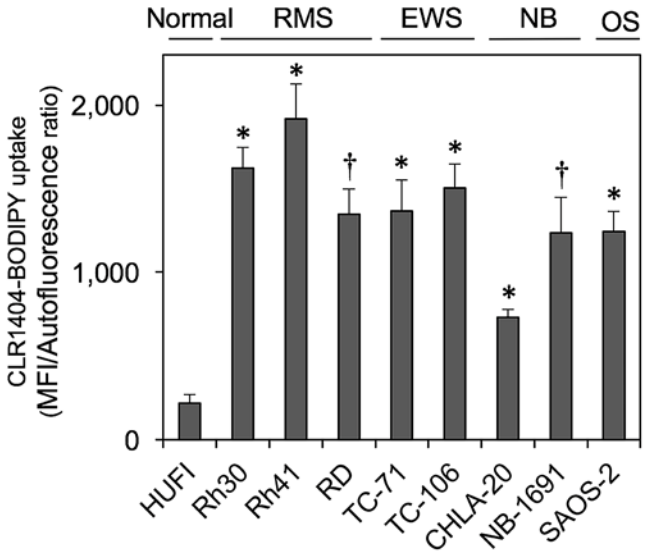

FIGURE 1. Preferential uptake of CLR1404 by pediatric solid cancer cells, compared to normal human fibroblasts (HUFI), by flow cytometry. Mean ± standard error from minimum 3 experiments per cell line, **P* < 0.01; †*P* < 0.05. EWS, Ewing's sarcoma; MFI, mean fluorescence intensity; NB, neuroblastoma; OS, osteosarcoma; RMS, rhabdomyosarcoma.

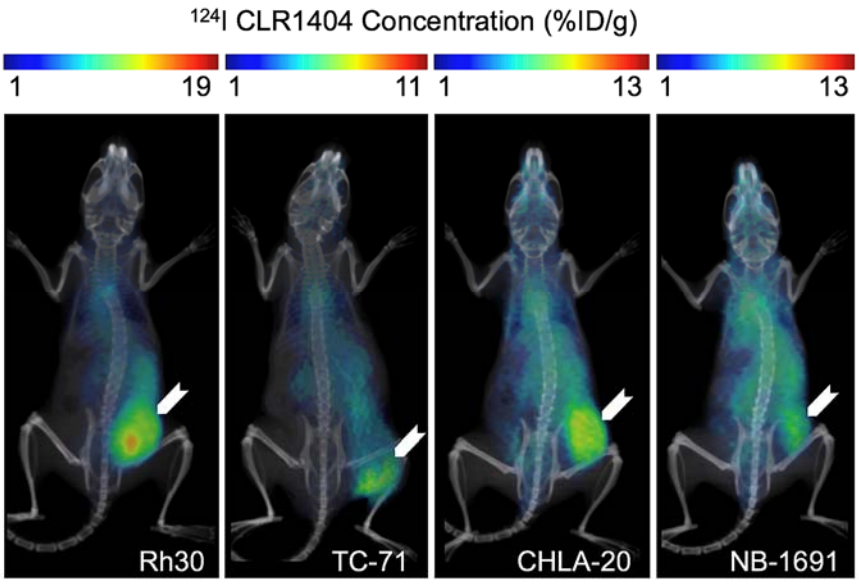

FIGURE 2. Colorwashes of tissue activity calculated as percent of injected dose/g tissue (%ID/g) in xenografts (arrowheads) and normal tissues of NSG mice, 72h after ^{124}I-CLR1404 administration. Shown are coronal MicroPET/CT three-dimensional volume renderings of one representative mouse of four scanned for each tumor type.

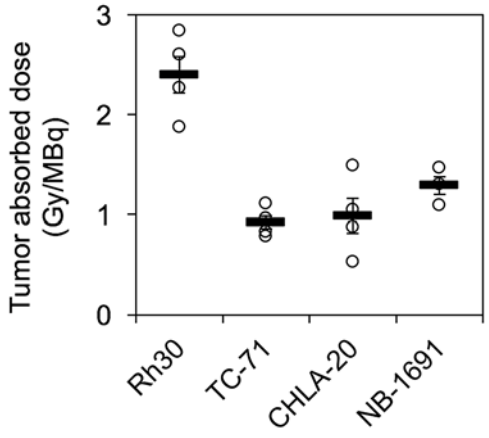

FIGURE 3. Calculated ^{131}I-CLR1404 absorbed dose per individual mouse xenograft (circles) and mean (horizontal bar) ± standard error. Each circle represents one mouse (n=4).

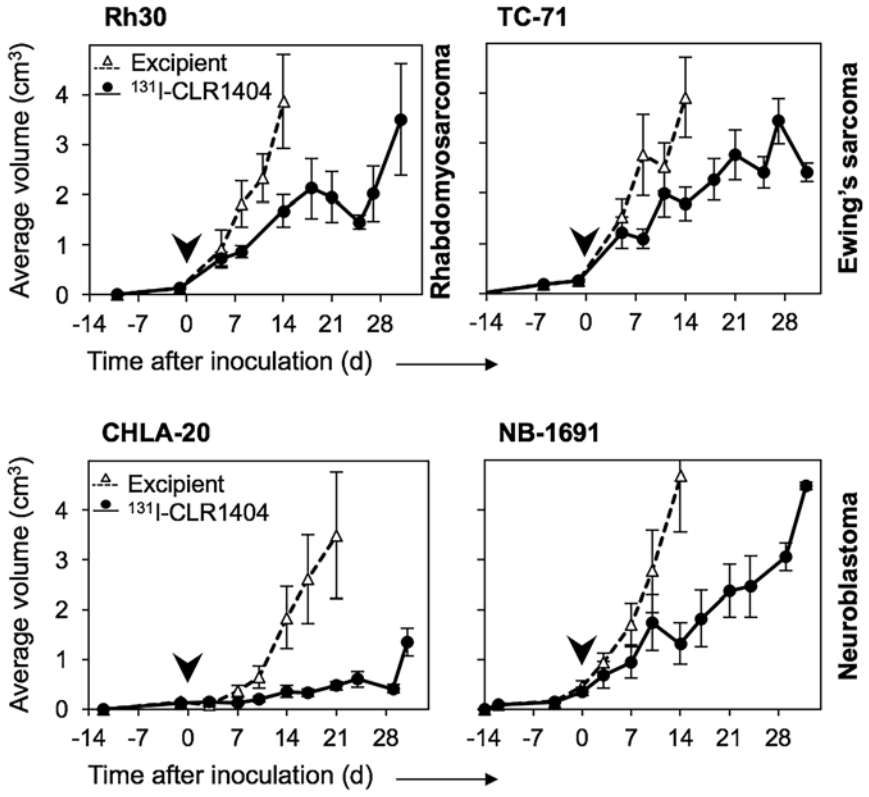

FIGURE 4. Radiotherapeutic effect of ^{131}I-CLR1404 in pediatric solid cancer xenograft NSG models, versus excipient. Mean ± standard error tumor volumes for the duration of four ^{131}I half-lives. Arrowhead, start of treatment; d, days. Number of animals detailed in Table 1.

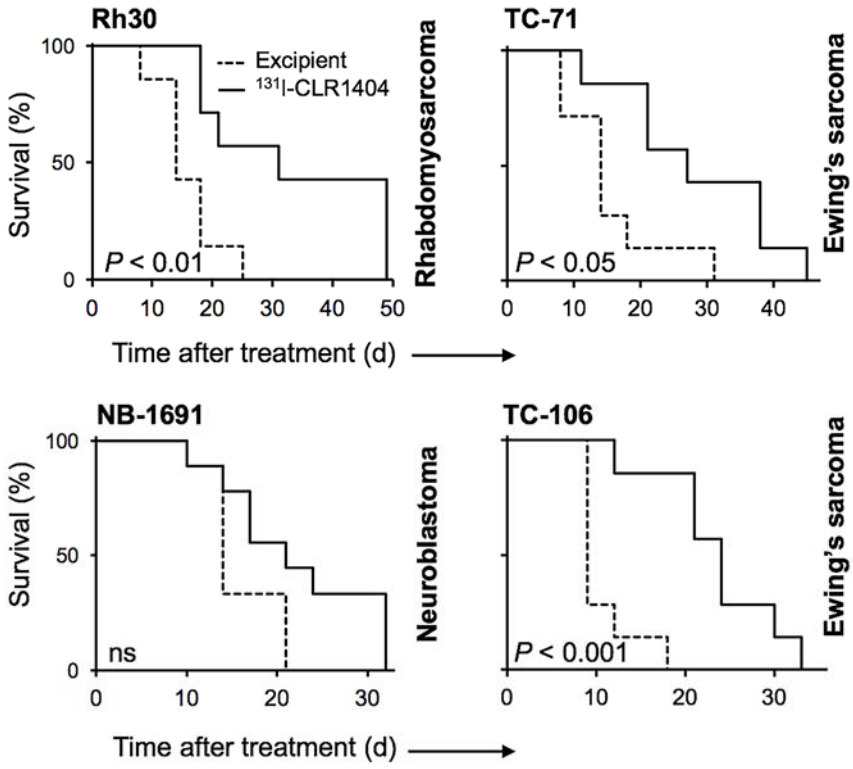

FIGURE 5. Kaplan-Meier survival analysis in pediatric xenograft models after administration of ^{131}I-CLR1404. d, days; ns, not significant. Number of animals detailed in Table 1.

TABLE 1
Tumor Growth Rate Analysis Using a Linear Mixed Effects Model

Xenograft	*n* animals/ experiment	*n* animals/ group	Slope log volume*		*P* value†
			Excipient	^{131}I –CLR1404	
Rh30	14	7	0.18	0.06	<0.0001
TC-71	14	7	0.14	0.08	<0.0003
TC-106	14	7	0.26	0.10	<0.0001
CHLA-20	12	6	0.13	0.09	0.0124
NB-1691	18	9	0.15	0.09	<0.0001
SAOS-2	14	7	0.11	0.08	<0.0001

*Prediction of the tumor growth rate (slope of the mixed model function, using logarithmic transformation of tumor volumes).

†Comparison between predicted tumor growth rates of excipient versus drug treatment group.

SUPPLEMENTAL INFORMATION

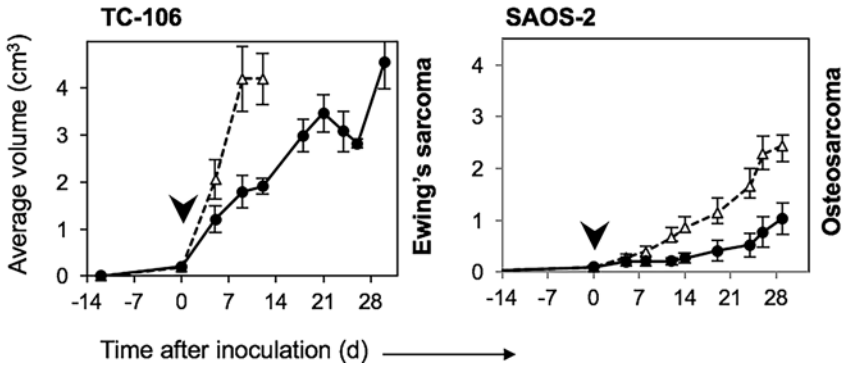

SUPPLEMENTAL FIGURE 1. Radiotherapeutic effect of ^{131}I-CLR1404 in pediatric solid cancer xenograft NSG models, versus excipient: mean ± SE tumor volumes for the duration of four ^{131}I half-lives. Arrowhead, start of treatment; d, days. Number of animals detailed in Table 1.

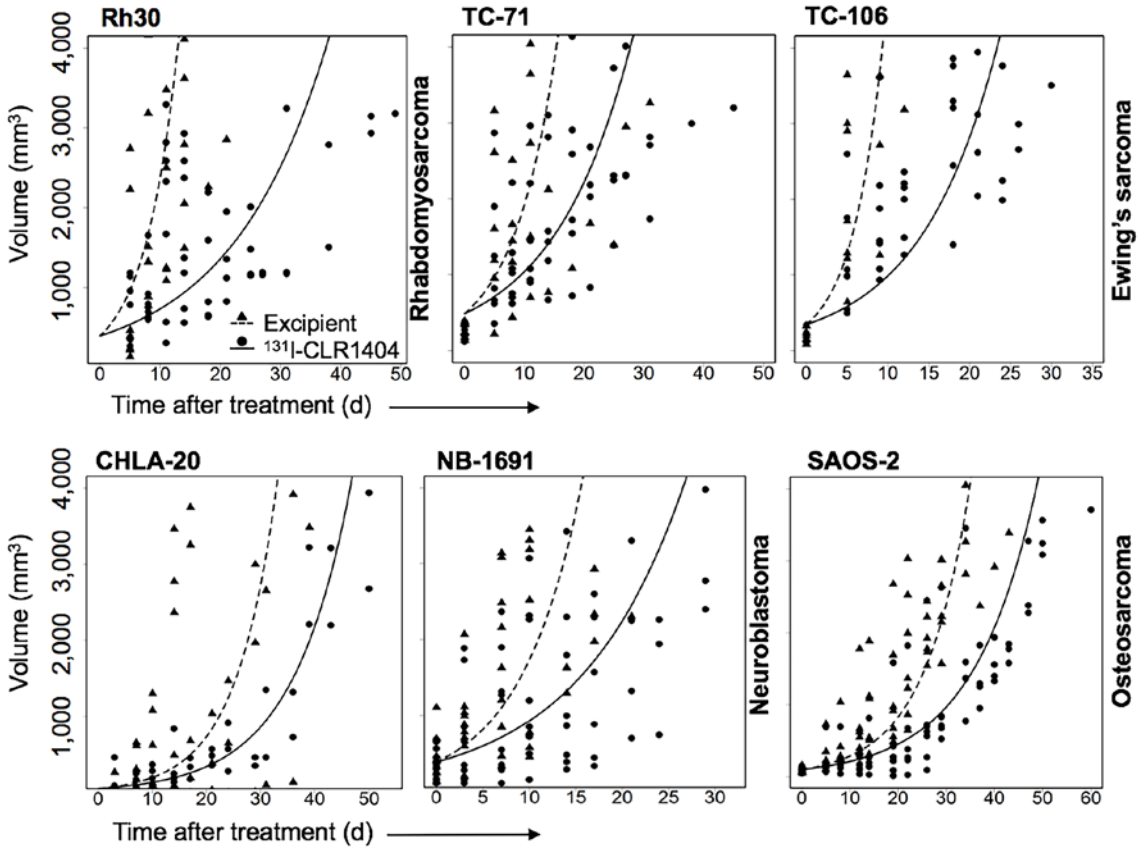

SUPPLEMENTAL FIGURE 2. Radiotherapeutic effect of ^{131}I-CLR1404 in pediatric solid cancer xenograft NSG models, versus excipient: linear mixed effects analysis of predicted growth rate (each symbol represents one mouse/time-point). d, days. Number of animals detailed in Table 1.

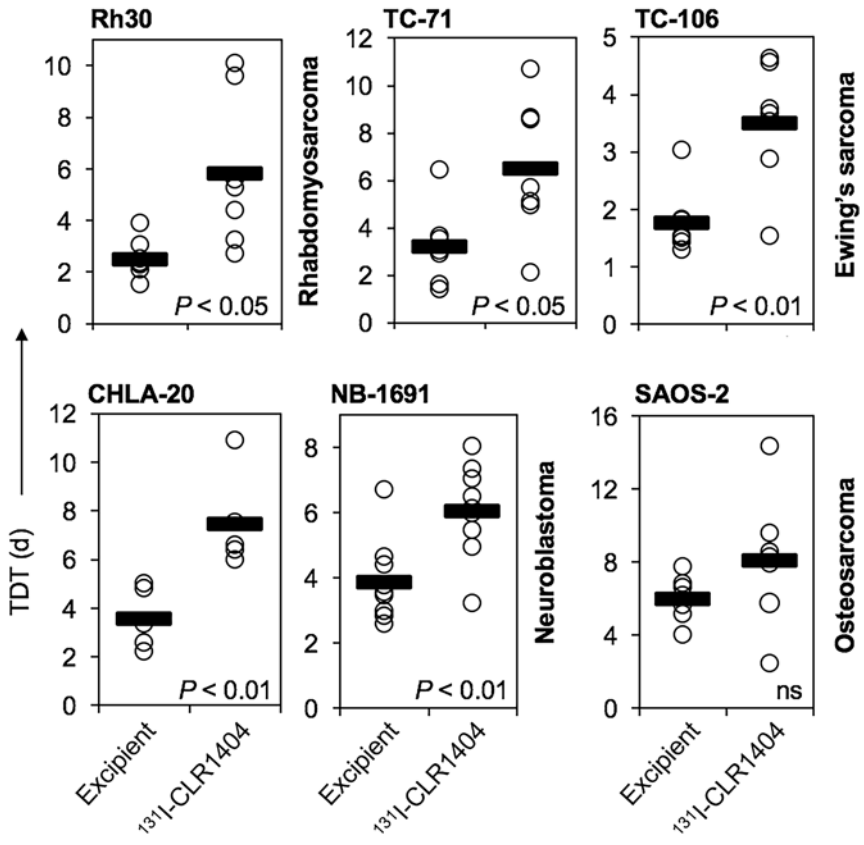

SUPPLEMENTAL FIGURE 3. Tumor doubling time (TDT) of xenografts after treatment with ^{131}I-CLR1404 or excipient (mean ± SE). Each symbol represents an individual mouse; ns, not significant. Number of animals detailed in Table 1.

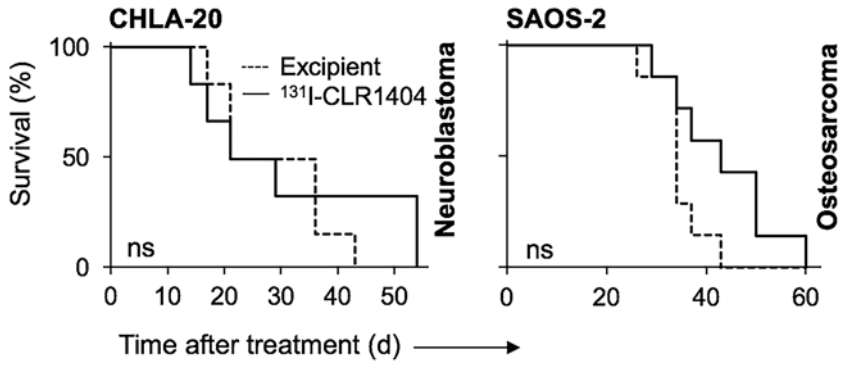

SUPPLEMENTAL FIGURE 4. Kaplan-Meier survival analysis in pediatric sarcoma xenograft models after administration of ^{131}I-CLR1404. d, days; ns, not significant. Number of animals detailed in Table 1.

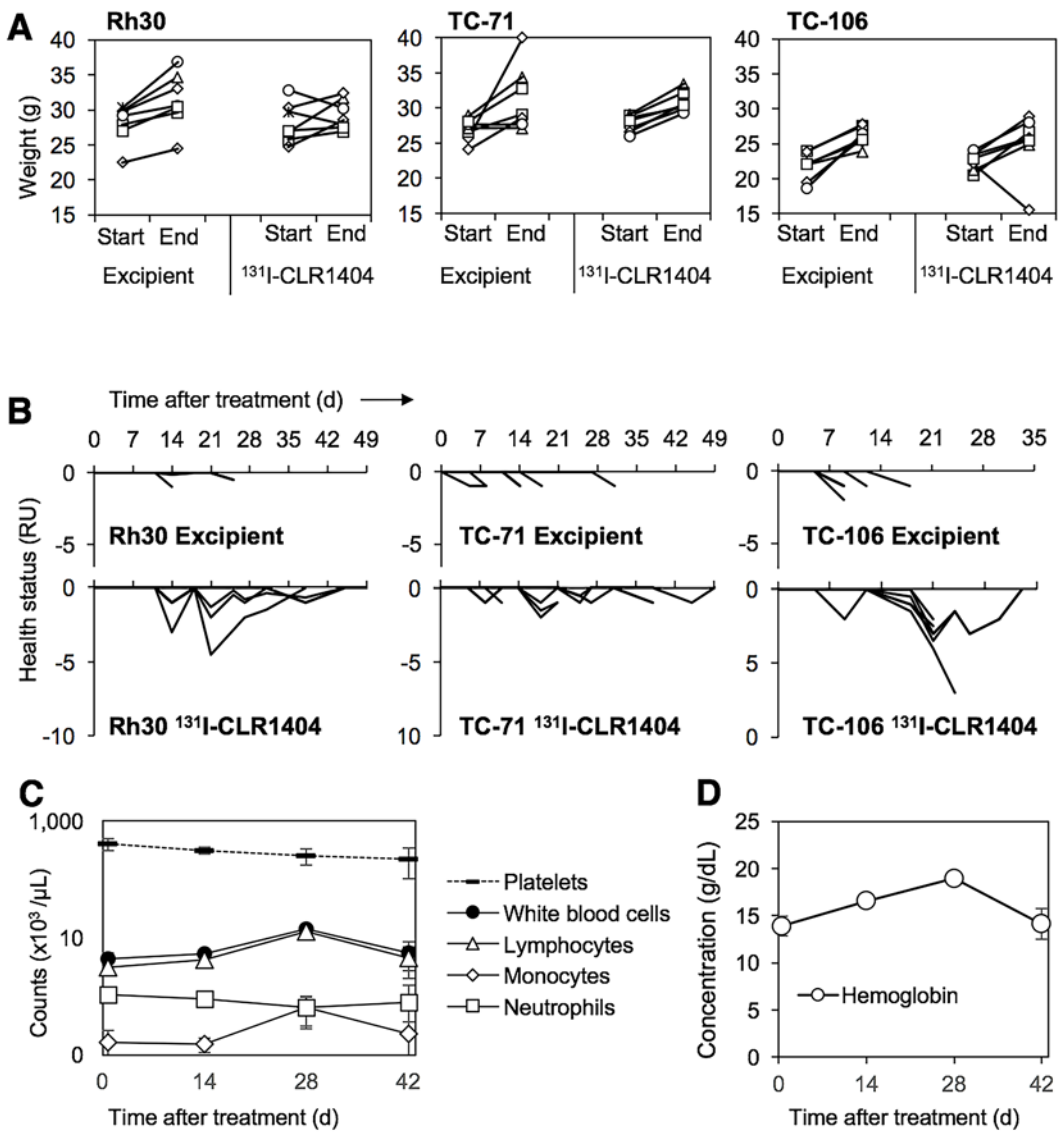

SUPPLEMENTAL FIGURE 5. Evaluation of radiotherapy-associated toxicity. Body weight variation in experimental window (A), and cumulative health score (B), in pediatric sarcoma NSG xenograft models after administration of ^{131}I-CLR1404 (n=7/group). Counts of blood cells (C) and hemoglobin concentration (D), after administration of ^{131}I-CLR1404 in BALB/c mice (mean ± SE, n=5). d, days; RU, relative units.

SUPPLEMENTAL TABLE 1

Physical Characteristics of the Radiolabeled Products

Radioiodinated product	Radionuclide provider	Physical T½*	Beta energies†	Gamma or X energies†	Electrons energies†
^{124}I-CLR1404	IBA Molecular (St. Louis, MO)	4.18	1,532 (11) 2,135 (11) 810 (< 1)	511 (46) 603 (61) 1,691 (11)	23 (8) 571 (< 1)
^{131}I-CLR1404	Perkin Elmer, (Waltham, MA)	8.04	248 (2) 334 (7) 606 (90)	284 (6) 365 (82) 637 (7)	46 (4) 330 (2)

*T½, half-life, in days.

†Main emissions, in keV; numbers in parentheses are decay percentages (*1*).

SUPPLEMENTAL TABLE 2

Activity Concentrations in Tissues of Rh30 Rhabdomyosarcoma Xenografted Animals

Organ	Mean %ID/g ± SD as a function of time				
	T1* (0.4 h)	T2 (25 h)	T3 (48 h)	T4 (72 h)	T5 (169 h)
Brain	2.1 ± 0.2	1.5 ± 0.3	1.6 ± 0.3	1.6 ± 0.2	1.6 ± 0.2
Cord	4.3 ± 0.4	3.0 ± 0.2	3.1 ± 0.4	2.9 ± 0.5	2.6 ± 0.3
Lungs	8.5 ± 0.6	4.2 ± 0.4	3.9 ± 0.5	3.5 ± 0.5	2.8 ± 0.4
Heart	17.9 ± 1.8	7.2 ± 0.8	6.9 ± 1.1	6.3 ± 1.0	5.0 ± 0.8
Kidneys	8.0 ± 0.3	5.6 ± 0.2	5.0 ± 0.4	4.8 ± 1.0	3.2 ± 0.5
Liver	10.6 ± 1.5	5.8 ± 0.6	5.1 ± 0.7	4.7 ± 0.7	3.4 ± 0.5
Marrow	3.4 ± 0.2	3.4 ± 0.3	3.3 ± 0.4	3.2 ± 0.4	2.7 ± 0.3
Tumor	1.1 ± 0.2	6.4 ± 0.7	7.2 ± 1.1	7.5 ± 1.4	7.2 ± 1.5

*T1-T5, time points of PET/CT imaging

SUPPLEMENTAL TABLE 3

Activity Concentrations in Tissues of TC-71 Ewing's Sarcoma Xenografted Animals

Organ	Mean %ID/g ± SD as a function of time				
	T1* (0.3 h)	T2 (25 h)	T3 (48 h)	T4 (72 h)	T5 (170 h)
Brain	1.8 ± 0.3	1.3 ± 0.1	1.4 ± 0.2	1.4 ± 0.2	1.2 ± 0.2
Cord	3.3 ± 0.5	2.5 ± 0.5	2.5 ± 0.4	2.5 ± 0.8	2.1 ± 0.5
Lungs	7.5 ± 2.4	3.6 ± 1.0	3.4 ± 1.3	3.1 ± 1.5	2.5 ± 1.4
Heart	16.0 ± 2.8	6.7 ± 1.1	6.4 ± 1.3	5.9 ± 1.5	4.5 ± 0.7
Kidneys	6.6 ± 0.5	4.7 ± 0.7	4.3 ± 0.9	4.9 ± 1.3	2.9 ± 0.4
Liver	9.3 ± 1.2	5.3 ± 0.9	4.8 ± 1.2	4.9 ± 1.3	3.2 ± 0.5
Marrow	2.7 ± 0.5	2.9 ± 0.5	2.8 ± 0.4	3.0 ± 0.5	2.6 ± 0.3
Tumor	0.9 ± 0.6	3.5 ± 1.0	3.5 ± 0.9	3.2 ± 0.7	2.5 ± 0.3

*T1-T5, time points of PET/CT imaging

SUPPLEMENTAL TABLE 4

Activity Concentrations in Tissues of CHLA-20 Neuroblastoma Xenografted Animals

Organ	Mean %ID/g ± SD as a function of time				
	T1* (2 h)	T2 (23 h)	T3 (46 h)	T4 (70 h)	T5 (96 h)
Brain	1.6 ± 0.1	1.6 ± 0.2	1.7 ± 0.1	1.6 ± 0.2	1.8 ± 0.2
Cord	3.6 ± 0.2	3.5 ± 0.4	3.6 ± 0.6	3.4 ± 0.1	4.0 ± 0.9
Lungs	6.2 ± 0.3	5.1 ± 0.7	4.8 ± 0.5	4.4 ± 0.3	4.4 ± 0.4
Heart	12.2 ± 1.4	8.4 ± 0.6	7.9 ± 0.5	7.7 ± 0.2	7.8 ± 0.4
Kidneys	7.3 ± 0.7	6.7 ± 1.0	6.4 ± 0.9	5.8 ± 0.8	6.1 ± 1.1
Liver	9.3 ± 1.1	7.0 ± 0.7	6.2 ± 0.5	6.0 ± 0.5	6.0 ± 0.6
Marrow	3.2 ± 0.4	3.6 ± 0.9	4.0 ± 1.4	3.8 ± 1.0	3.5 ± 0.7
Tumor	2.9 ± 1.1	5.6 ± 2.3	5.6 ± 2.5	5.0 ± 2.2	4.5 ± 2.1

*T1-T5, time points of PET/CT imaging

SUPPLEMENTAL TABLE 5

Activity Concentrations in Tissues of NB-1691 Neuroblastoma Xenografted Animals

Organ	Mean %ID/g ± SD as a function of time				
	T1* (3.5 h)	T2 (24 h)	T3 (46 h)	T4 (71 h)	T5 (97 h)
Brain	1.6 ± 0.4	1.6 ± 0.2	1.6 ± 0.3	1.5 ± 0.4	1.6 ± 0.3
Cord	3.4 ± 0.8	3.3 ± 0.5	3.2 ± 0.6	3.1 ± 0.8	3.1 ± 0.5
Lungs	5.7 ± 1.2	4.6 ± 0.5	4.1 ± 0.5	3.9 ± .09	3.8 ± 0.7
Heart	10.6 ± 2.2	8.2 ± 1.2	7.5 ± 1.4	6.9 ± 1.9	7.0 ± 1.5
Kidneys	6.3 ± 1.1	6.1 ± 0.7	5.3 ± 0.5	4.8 ± 0.9	4.5 ± 1.4
Liver	7.8 ± 1.4	6.0 ± 0.9	5.1 ± 0.9	4.8 ± 1.5	4.9 ± 1.2
Marrow	3.4 ± 0.9	3.7 ± 0.9	3.6 ± 0.9	3.4 ± 1.0	3.5 ± 0.8
Tumor	2.6 ± 0.6	4.5 ± 1.3	4.6 ± 1.3	4.1 ± 1.2	3.8 ± 0.7

*T1-T5, time points of PET/CT imaging

REFERENCES

1. Delacroix D, Guerre JP, Leblanc P, Hickman C. Radionuclide and radiation protection data handbook 2002. *Radiat Prot Dosimetry.* 2002;98:5-168.